Chapter 2

Synthesis and Experimental Techniques

2.1 Introduction

This chapter presents a thorough examination of the methodology utilized in the present study, including the preparation of the samples and the diverse characterization techniques applied. The standard arc melting furnace method was utilized for sample preparation. Following this, a concise description of the operational principles and experimental configurations of various characterization instruments utilized to quantify distinct properties of as-prepared systems is provided. This includes X-ray diffraction for phase confirmation, a magnetic properties measurement system (MPMS) for magnetization measurements, a homemade setup for thermoelectric measurement, and a physical properties measurement system (PPMS) for assessing magnetotransport properties like Hall effect and magnetoresistance.

2.2 Material Synthesis Techniques

2.2.1 Arc Melting method

The samples chosen for this study were prepared utilizing the standard vacuum arc melting technique, which is frequently applied to produce polycrystalline specimens of intermetallic compounds and alloys. Throughout the melting procedure, a regulated inert atmosphere was upheld within the vacuum arc furnace. The samples were melted in the crucible of a copper (Cu) hearth cooled with water, which served as the anode. Concurrently, the melting process was aided by a water-cooled tungsten point that functioned as the cathode and was connected to the power supply (199 A, 18 V; INTIG-250IDS Inverter Welder).

The Cu-hearth, which consisted of four crucibles, enabled the melting of multiple samples simultaneously. The uniform heat distribution within the Cu-hearth was facilitated by copper's high thermal conductivity, which effectively averted localized melting. In contrast, the efficient emission of electrons was enabled by the low work function of tungsten, which promoted the generation of arcs at low power. The arc, induced between the tungsten tip and Cu-hearth in the presence of argon (Ar) gas at a pressure of approximately one psi, with 60 to 80 Amperes at 12 Volts constituting typical operating conditions. The high current density made possible by the tungsten cathode's tip shape resulted in the formation of plasma (or an arc) as electrons moved from the Ar gas to the anode. The temperatures generated by this arc were around 3000 ºC, which were adequate to melt the majority of metallic elements. The subsequent procedure for melting is described in detail below.

The raw materials, boasting a purity exceeding 99.99 %, were meticulously weighed using a Denver Instruments electronic balance. These precisely measured raw materials were then placed in a Cu-crucible within the arc furnace chamber alongside a titanium (Ti) ball housed in another Cu-crucible. Subsequently, the arc furnace chamber underwent

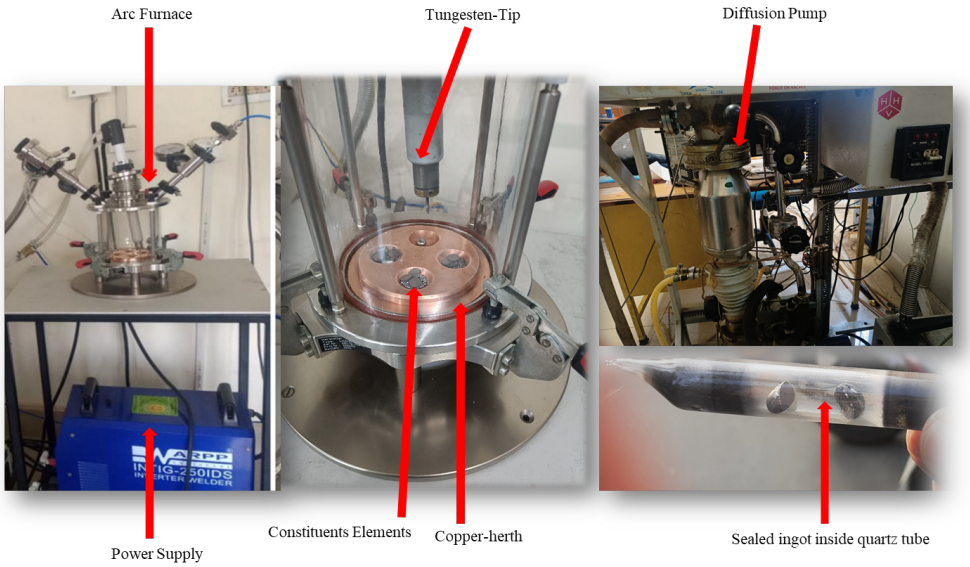

Fig. 2.1 arrangement of vacuum arc melting furnace and image of melted ingot sealed inside the quartz tube.

evacuation, reaching a minimum vacuum level on the order of 10^{-3} mbar through the operation of a rotary pump. Following evacuation, the chamber underwent purging by filling with argon (Ar) gas up to atmospheric pressure, followed by repeated evacuations. The use of Ar gas, with its heavier molecules, facilitated the removal of air molecules from the chamber. Typically, this purging process was repeated 4-5 times to establish an effective inert atmosphere, crucial for preventing oxidation of metallic materials during the melting process. Following purging, Ar gas was introduced to a pressure of 1 psi, initiating the arc through the power supply. Initially, titanium (Ti) was melted to reduce air molecules within the chamber, given its high reactivity and susceptibility to oxidation. Subsequently, the raw materials were melted to form the sample, with the melting process iterated 3-4 times, involving flipping the sample to ensure a homogenous composition. Mass measurements taken before and after melting revealed a weight loss below 1% for all prepared samples. The resulting button-shaped ingot, or sample, was further annealed for homogeneity. This involved eloping the ingot in a sealed quartz ampoule and evacuating the ampoule to a vacuum of 10^{-6} mbar using a diffusion pump. The image of Arc-melting

furnace along with the vacuum pump is shown in figure 2.1. The vacuum-sealed quartz ampoule underwent annealing in the furnace at the specified temperature and duration, dependent on the composition. Finally, the vacuum-sealed ingot was either quenched or slowly cooled to room temperature to attain the desired ordered phase. figure 1.3 provides a visual representation of the arc-melting furnace alongside the vacuum-sealing setup employed in the sample preparation for this study.

2.2.2 Muffle furnace

A muffle furnace is used to provide heat treatment to the system. The name of the device is derived from the refractory material, known as a muffle, which encloses the heating element and serves to shield the item being heated from direct contact with the flame or electric heating element. The working temperature of the furnace may reach up to 1800 °C, which is determined by its design and construction. Figure 2.2 displays the visual representation of the muffle furnace located in our laboratory. The maximum working temperature is 1300 °C. It has a digital temperature controller that allows for programming the desired settings.

2.3 Experimental Characterization Tools

2.3.1 X-Ray Diffraction (XRD)

XRD is a quick, non-destructive analytical method primarily utilized to determine the phase formation of the system. The fundamental principle behind XRD lies in the interaction of X-rays with a crystalline sample. A simplified explanation of the working principle of XRD is discussed here; The interaction between periodic structures and electromagnetic radiation results the diffraction phenomenon. X-rays possess high energy due to their very short wavelength of the order of few Angstroms (1 Angstrom = 0.1 nm). When a monochromatic

X-ray beam is directed at a sample, the X-ray photons within it engage with the electrons of atoms in the sample. Consequently, some photons undergo diffraction, deviating from their original incident trajectory. Diffraction manifests when electromagnetic waves bend around an obstacle, especially when the obstacle's size is comparable to the wavelength of the wave. In crystalline materials, where inter-atomic distances fall within the range of 1 to 10 Å (similar to the order of X-ray wavelength), In crystals, atoms are arranged in a periodic fashion. If the interference resulting from diffracted waves adheres to Bragg's condition, it produces the X-ray diffraction pattern for a given material. This pattern is discerned by measuring the intensity of diffracted waves across various incident angles of the X-ray. The XRD pattern, thus obtained, is a rich source of information. Essentially, by analyzing the XRD pattern, researchers have insights into the crystal structure and dimensions of the unit cell.

W. Lawrence Bragg and William H. Bragg formulated the law governing the diffraction of X-rays from crystalline planes, commonly referred to as Bragg's law Cullity & Stock (2001). Bragg's law serves to clarify the correlation between the angle at which the X-ray beam diffracts from the crystalline structure and the wavelength employed for X-rays. This relationship can be articulated as:

$$2d \sin\theta = n\lambda \tag{2.1}$$

In Bragg's law, where "n" represents the diffraction order, "λ" is the X-ray wavelength utilized, "d" signifies the interplanar distance between atoms, and "θ" denotes the scattering angle or Bragg's angle. The process involves recording the intensity of diffracted X-rays as a function of the Bragg angle (2θ). To carry out this measurement, the Rigaku-Miniflex II DESKTOP powder X-ray diffractometer, depicted in figure 2.3, was employed. This diffractometer features a monochromatic X-ray source emitting Cu-Kα radiation (λ =

1.5418 Å) at 30 kV and 15 mA. The recorded data provides valuable insights into the intensity variation with the Bragg angle, aiding in the analysis of the crystalline structure and interatomic distances in the studied material.

2.3.2 X-ray Photoemission spectroscopy (XPS)

The XPS is a technique used to analyze the elemental composition of a material and to study its electronic properties. This includes a profound examination of oxidation states, elemental composition, ligand coordination, and more. Notably, XPS extends its investigative reach to both insulators and conductors, covering surface areas ranging from a few microns to a few millimeters in depth.

- **Working Principle:**

For the XPS spectra, the system is exposed to a low energy monochromatic X-ray source under an ultrahigh vacuum environment typically $10^{-10} torr$. The incident X-rays initiate the ejection of electrons at the core level from the atoms of the sample. Indeed, the energy of a core electron generated through photoemission is an attribute of the element from which it was emitted and is proportional to its binding energy. The fundamental information utilized in XPS is the energy analysis of the electrons that are emitted during photon emission. An exterior electron is introduced into the core cavity when the incident X-ray ejects the core electron. These energies are offset through the emission of a characteristic X-ray or Auger electron. Moreover, in XPS Auger, the energy of electrons emitted in addition to photoelectrons can be utilized. The energy of individual photoelectrons is calculated using the equation proposed by Ernest-Rutherford in 1914:

$$E_{kinecticenergy} = h\nu - (E_B + \phi) \tag{2.2}$$

Here, E_B is the binding energy of the electron, $h\nu$, represents the energy of the incident X-ray photons, $E_{Kineticenergy}$ represents the kinetic energy of the electron and ϕ is the work function of the spectrometer. This is represented in figure2.4. Figure 2.4 elucidates the diverse instrumental units comprising an XPS machine as;

1. Hemispherical electron energy analyzer
2. X-ray source
3. Ar-ion gun
4. Vacuum system
5. Neutralizer or electron flood gun
6. Multi-channel detector plates
7. Sample stage or holder
8. Electronic control units
9. Computer

2.3.3 Raman Spectroscopy

Raman spectroscopy is a powerful analytical technique used to study vibrational, rotational, and other low-frequency modes in a system. Named after the Indian physicist Sir C.V. Raman who discovered the effect in 1928, Raman spectroscopy provides valuable information about molecular vibrations and the structure of materials. Raman and his research partner Krishan made a groundbreaking discovery in 1928. Their initial experimentation involved sunlight as a source and the naked eye as a detector, reflecting the limited instrumentation of the time.

Progressively, advancements occurred, transitioning from the use of a photographic plate to the invention of sophisticated excitation sources and detectors. The evolution culminated in the accessibility of commercial Raman spectrometers. This technique, a pioneer in probing the qualitative and quantitative dynamics of atoms, ions, and molecules in crystals through light scattering, underwent a transformative journey. In the Raman effect, the majority of photons experience elastic scattering, retaining the same energy as the incident photons—a phenomenon known as Rayleigh scattering. In a minute fraction of cases, about 1 in 10^7 photons, inelastic scattering occurs, resulting in a change in wavelength due to alterations in rotational, vibrational, or electronic energy—the essence of the Raman shift as shown in figure 2.5. The Raman effect can be elucidated by considering the deformation of molecules in an electric field. The induced electric dipole moment ($P = \alpha$ where α is polarizability) in this field gives rise to the Raman shift, observed only when the derivative of α is nonzero concerning normal coordinates (Q).

When electromagnetic radiation interacts with atoms or molecules, their electron clouds and bonds undergo distortion. This interaction propels the entities to a virtual energy state, rendering them temporarily unstable. The return to a different stable state, whether rotational or vibrational, involves the release of a photon, resulting in a shift in frequency—termed the Raman shift—from the excitation energy. The Raman spectra, typically expressed in wave numbers (cm^{-1}), detail the frequency shifts. In practical applications, a Renishaw Raman spectrometer equipped with a diode-pumped solid-state laser emitting light at 532 nm was utilized. To prevent specimen heating, only 5 percent of the laser power was incident on the sample. The laser beam, focused with a 50 $\times$ long-distance objective connected to a Leica DM 2500M microscope, underwent dispersion via a grating with 2400 grooves/mm and a 50-micron slit width. The scattered light was collected and transmitted to a detector, and data processing ensued using the provided 4.0 software for spectrometer scanning. we employed the temperature-dependent Raman spectroscopy

technique with a LabRam HR Evolution spectrometer manufactured by Horiba. This advanced spectroscopic tool allows us to explore how vibrational characteristics evolve under varying conditions.

2.3.4 X-ray absorption spectroscopy (XAS)

The X-ray absorption spectroscopy studies involve two main techniques: X-ray Absorption Spectroscopy (XAS) and X-ray Photoelectron Spectroscopy (XPS). These methods explore transitions related to the absorption and emission of X-rays, respectively. XAS focuses on ground state to excited state transitions, while XPS investigates the decay process from the excited state. Despite their differences, both techniques effectively probe the chemical states and local environments of atoms in molecules. In XAS, incident X-ray photons excite electrons in the core level to unoccupied conduction levels, following the intra-atomic dipole selection rule. This technique is element-specific, as the energy difference between the core and conduction levels is unique to each element. Synchrotron-based XAS, a spectroscopic tool for probing electronic states, offers a broad range of X-ray energies capable of detecting most elements in the periodic table. Unlike other methods, such as optical absorption or fluorescence, XAS relies on a chosen X-ray energy to identify the specific element being examined.

Over the past few decades, XAS has gained popularity due to its element specificity, sensitivity to spin orientation, and surface sensitivity. Similar to XPS, XAS facilitates quantitative analysis of element oxidation states. However, it also possesses the intrinsic ability to sense magnetic ordering. Circular polarization of synchrotron X-rays enables the investigation of the spin orientation of magnetic materials. Information about magnetic ordering is embedded in the same multiplet structure used to identify different chemical species. The presence of ferromagnetic (FM) or antiferromagnetic (AFM) ordering manifests as changes in peak intensities and energy positions within the multiplet pattern.

Understanding both the shape of spectra representing a specific element and potential alterations accompanying different magnetic orderings is crucial. This knowledge allows the extraction of magnetic information not only for a specific element but also for different chemical phases of that element. The schematic diagram of XAS spectra, as illustrated in figure 2.6, reveals sharp rises in absorption at specific X-ray photon energies, known as absorption edges. These edges, such as the K-edge for 1s core level ionization or the L-edge for 2s or 2p electron ionization, are characteristic features of the absorbing element. Similarly, the M-edge corresponds to photoelectrons exciting from 3s/3p/3d electrons. In the present thesis, the XAS spectra transition metal elements is performed.

2.3.5 X-ray magnetic circular dichroism (XMCD)

X-ray Magnetic Circular Dichroism (XMCD) spectroscopy involves comparing two XAS spectra derived from left and right circularly polarized light, both in the presence of a magnetic field. This technique enables the extraction of vital information about the magnetic characteristics of atoms, specifically their spin and orbital magnetic moments. The contrast in spectra between parallel and anti-parallel light helicities is commonly referred to as XMCD. This innovative approach sheds light on the intricate magnetic properties of materials, offering valuable insights into their fundamental behavior and aiding advancements in fields such as condensed matter physics.

A schematic view of two beamlines XMCD experimental setup is illustrated in figure 2.7. The sample is positioned at the center of a superconducting magnet, which is illuminated with polarized and monochromatic X-rays. The magnetic field is applied along the direction of the incoming beam. To observe polarized-dependent X-ray Absorption Spectroscopy (XAS), two distinct techniques are employed: Fluorescence Yield (FY) and Total Electron Yield (TEY). Notably, TEY is commonly utilized in the soft X-ray spectral range. Fluorescence detectors, comprising single or multi-anode ion-implanted

silicon photodiodes, play a crucial role in this setup. These detectors are characterized by their remarkable attributes, including high efficiency within the X-ray range, rapid time response, outstanding linearity, and a nearly negligible sensitivity to the magnetic field. This comprehensive experimental arrangement enhances our ability to investigate and understand the magnetic properties of materials with precision.

2.3.6 Magnetic Property Measurement System (MPMS)

The magnetization measurements in our study have been performed using Quantum Design Magnetic Property Measurement system, i.e., "MPMS3" shown in figure 2.8. The allowed measurement condition for this system is shown in the list given below 2.9

Working Mechanism of SQUID

At the core of the MPMS lies the Superconducting Quantum Interference Device (SQUID) sensor, featuring two parallel Josephson Junctions, where two superconductors are separated by thin insulating (weak link) layers, as illustrated in figure 2.9. The theoretical foundation for the SQUID's operation was laid by B. D. Josephson in 1962. According to Josephson's effect, a supercurrent, reaching a maximum critical value (I_C), is generated and flows continuously through the weak link without any voltage across the Josephson junction, facilitated by the tunneling of Cooper pairs. Due to its superconducting ring structure, the SQUID only permits a magnetic flux through it in integral multiples of $\phi_0 = \frac{hbar}{e} = 2.07 \times 10^{-15} Tesla - m^2$, representing the flux quantization in superconductors. To maintain flux quantization, any alteration in the magnetic flux through the loop induces a screening current in the superconducting ring. The minute magnitude of ϕ_0 allows for the creation of an exceptionally sensitive magnetic sensor, such as the SQUID. Utilizing SQUIDs, the magnetic flux associated with any material can be converted into a voltage, leveraging the flux quantization sensitivity inherent in superconductors. An

external biased current applied through the SQUID prompts electron Cooper pairs to tunnel through the weak link junctions. When an external magnetic field from any material enters the ring, it modifies the critical current through the superconductor. This change in current is then amplified into a voltage signal using electronic instruments calibrated to provide the magnetic moment of the system. Consequently, the SQUID is also recognized as a flux-to-voltage transducer, capable of translating even minute changes in magnetic flux into a discernible voltage signal.

This system offers three distinct modes for conducting magnetization measurements:

- **DC Magnetization**

  Zero field cooling (ZFC) :

  This procedure is implemented when cooling the sample from room temperature to the lowest measurement temperature under a zero magnetic field. Subsequently, after applying the necessary magnetic field, data recording takes place as the sample is heated to the desired temperature.

  field cooling (FC) :

  This procedure is implemented when the sample is cooled from room temperature to the lowest measurement temperature while subjected to a magnetic field. Throughout this cooling cycle, data on M(T) are recorded.

- **AC Susceptibility** (χ_{ac}) **:** In addition to the previously mentioned DC measurements, we also conducted measurements of the real and imaginary parts of AC susceptibility (χ' and χ'' respectively) using the same instruments, varying both temperature (T) and frequency (f)

2.3.7 Transport Properties Measurements

- **Longitudinal Electrical Resistivity** (ρ_{xx}) **:** The electrical resistivity stands as a foundational aspect in material science, offering essential insights into the electronic properties and conductivity of various materials. Among the methods employed for such measurements, the four Probe Resistivity Setup is a precise technique. This setup assumes a crucial role in the comprehensive characterization of materials, particularly in assessing their electrical resistance. The experimental setup for four probe resistivity is shown in figure 2.10 (a). The ρ_{xx} of the synthesized systems was measured by the Physical Property Measurement System (PPMS) by utilizing the standard four-probe method. The resistivity of the system exhibits an inverse relationship with the length (l) between two voltage probes and a direct proportionality to the cross-sectional area (A). This mathematical relationship is expressed as:

$$\rho_{xx} = \frac{R.A}{l} \tag{2.3}$$

- **Transversy Electrical Resistivity (**ρ_{xy}**) :** The Hall resistivity is measured by altering the connection geometry as depicted in figure 2.10 (b). In this configuration, the voltage drop was measured across opposite surfaces of the sample, oriented perpendicular to both the applied current (I) and the external magnetic field (B).

- **Thermoelectric Measurement :** The determination of the Seebeck coefficient (S) involved a custom-made setup where the sample was positioned between two copper blocks. This sample holder assembly was affixed to a closed-cycle refrigerator (CCR), capable of controlled cooling from room temperature down to 20 K. To maintain a temperature difference of 2 K across the sample, a T-type thermocouple and two heater coils placed at both ends of the copper blocks were employed. The voltage difference (ΔV) between the cold and hot ends was precisely measured

using a Keithley 2182A nanovoltmeter, spanning from low temperatures to room temperature. The configuration of the sample holder assembly is visually represented in figure 2.11 This setup induces the diffusion of charge carriers from the hot end to the cold end, creating a thermal current. The Seebeck coefficient (S) is defined as the ratio of the magnitude of the induced thermoelectric voltage (ΔV) to the temperature difference (ΔT) across the sample and is expressed as:

$$S = \frac{(\Delta V)}{(\Delta T)} \tag{2.4}$$

Where, S is measured in $\mu V/K$, and its slope gives the nature of the transport carrier. A negative slope indicates the n-type nature of transport carriers in a sample, while the positive slope suggests the p-type nature of the transport carrier

Fig. 2.2 image of Muffle furnace with temperature controller

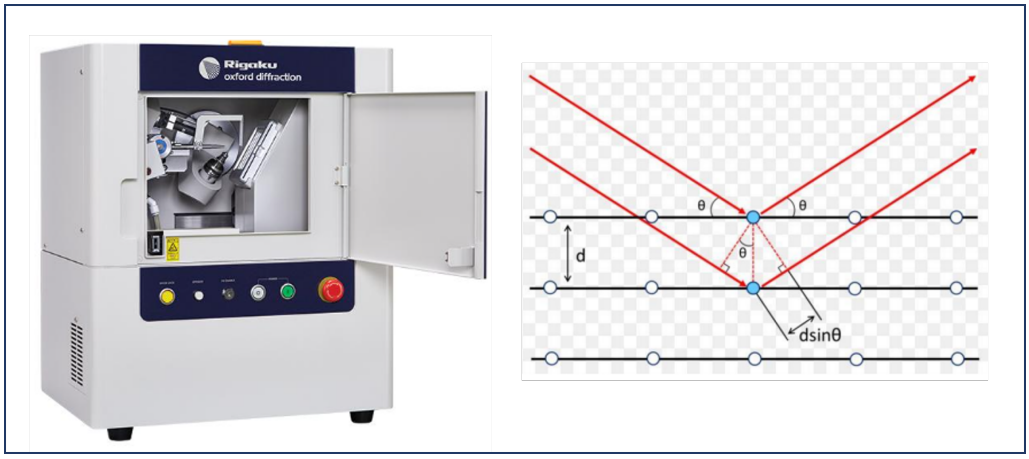

Fig. 2.3 X-ray Diffraction setup

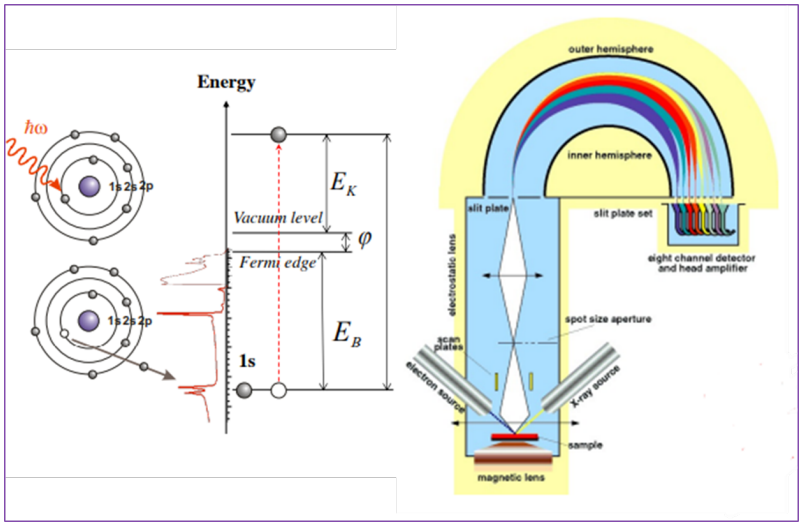

Fig. 2.4 Left Figure: Schematic diagram illustrating the photoelectric effect, capturing the essence of electron liberation in response to incident photons. Right Figure: Schematic diagram depicting the X-ray Photoemission Spectroscopy (XPS) setup.

[Source:http://https://engineering.purdue.edu/ yep/Lectures/XPS-UPS Auger]

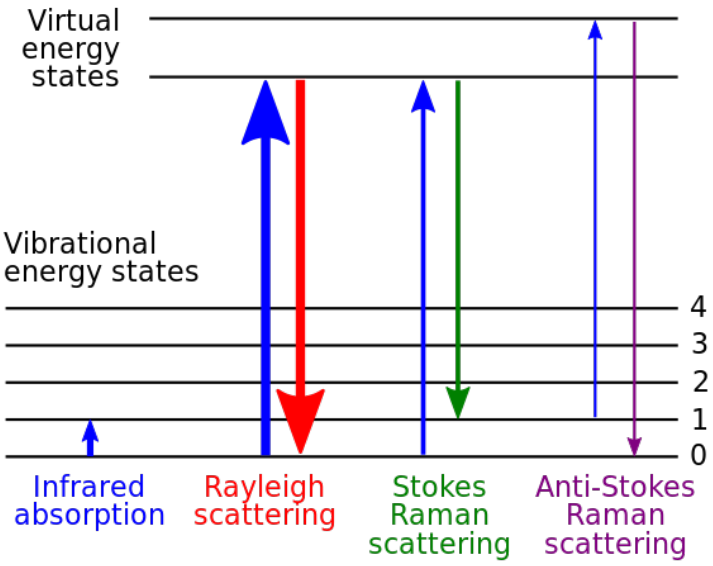

Fig. 2.5 Energy-level diagram showing the states involved in Raman spectra.

[Source:Raman spectroscopy.(2023, November 28). In Wikipedia. https://en.wikipedia.org/wiki/Raman spectroscopy]

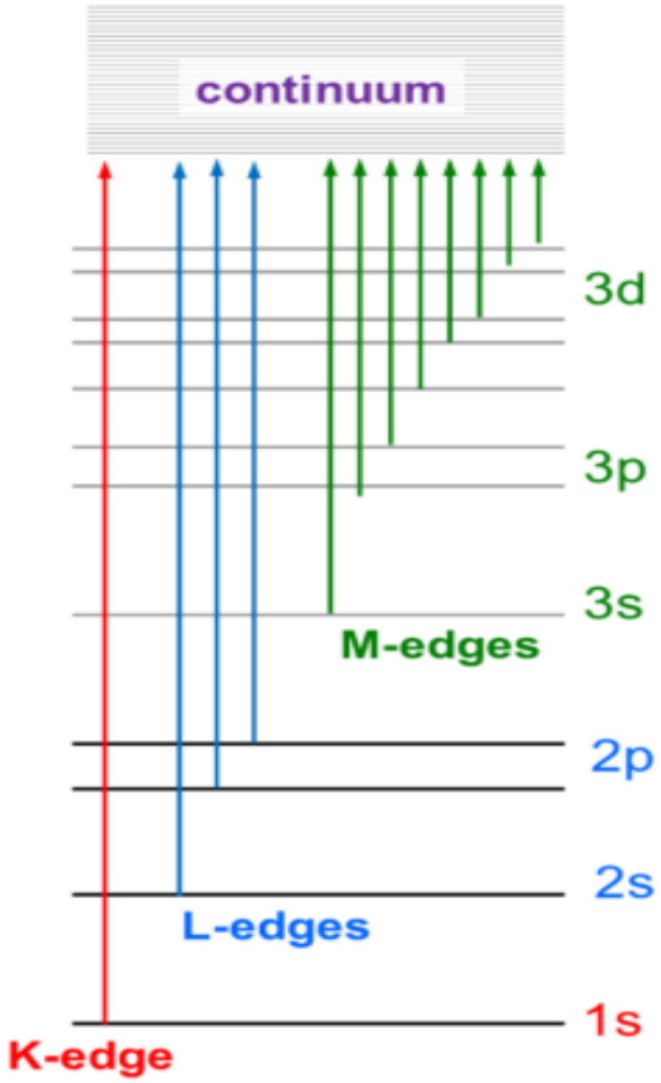

Fig. 2.6 Transitions between the core electron which rise near the XAS edges.

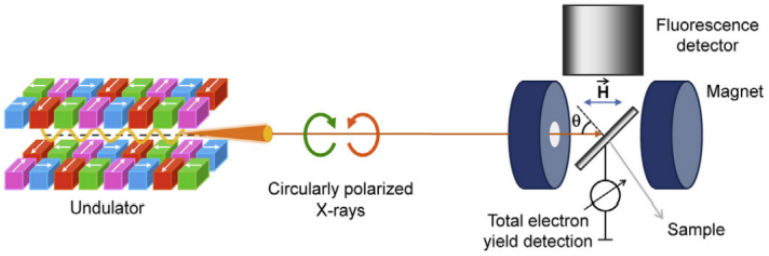

Fig. 2.7 Experimental setup for an XMCD experiment. The circularly polarized X-rays are provided by an undulator, which then irradiates the sample, which is kept magnetized by an applied magnetic field.

Source: van der Laan & Figueroa (2014)

Fig. 2.8 Image of Quantum design MPMS 3.

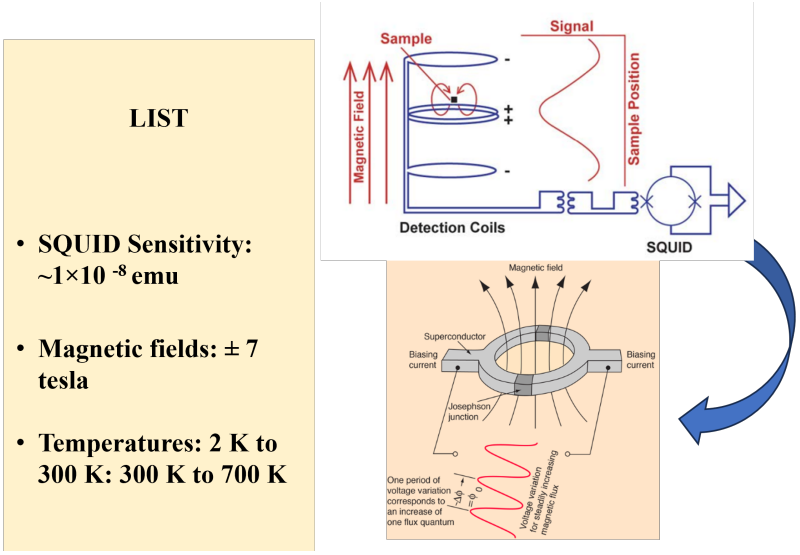

Fig. 2.9 MPMS 3 allowed conditions; Schematic representation of working principle of SQUID.

Source:http://hyperphysics.phy-astr.gsu.edu/hbase/Solids/Squid.html

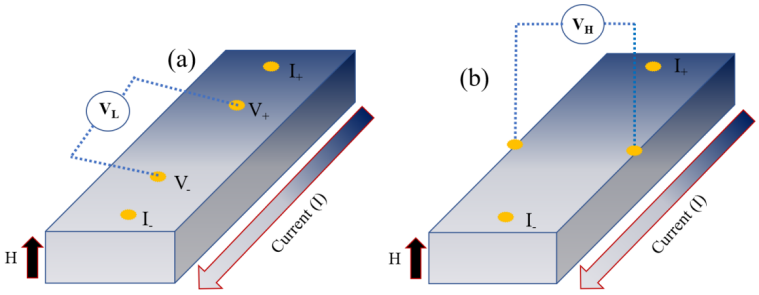

Fig. 2.10 (a) Schematic representation of longitudinal resistivity in four probe setup (ρ_{xx}). (b) Schematic representation of transverse resistivity (ρ_{xy})

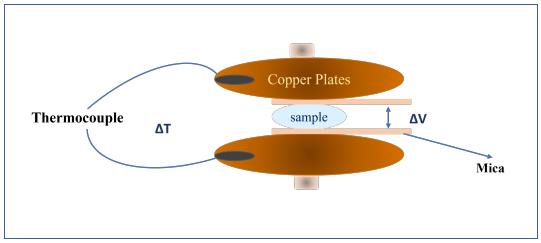

Fig. 2.11 Schematic diagram of sample holder for thermoelectric measurement